A state-space model for induction machine stator inter-turn fault and its evaluation at low severities by PCA

Krish K Raj, Sukhde H Joshi, Rahul Kumar*
School of Information Technology, Engineering, Mathematics and Physics
line 3: *The University of the South Pacific*
Suva, Fiji
*Email: rahul.kumar@usp.ac.fj

Abstract—**Early fault detection in rotating machines saves time, money and labor that must be spent repairing or replacing the machine caused by a abrupt breakdown while stopping the production process. Due to this reason, industries invest in routine maintenance, intending to diagnose faults and take preventive measures before the problem becomes severe. This paper presents a state-space model of the healthy and faulty induction motor. The fault considered in this study is the stator inter-turn fault, with the severity ranging from 0.3%-2.11% in a phase. This article gives an overview of the simulated model and shows how the healthy three-phase current signature is different from the faulty ones. The Principal Component Analysis (PCA) and Space Vector Loci (SVL), in particular, have been utilized to visualize and present the differences between the healthy and faulty current signatures. Furthermore, both PCA and SVL have also been instrumental in denoting minor fault severities.**

Keywords—Induction motor, Stator Inter-turn Fault, Principal Component Analysis, Space Vector Locus

I. Introduction

Induction Motor (IM) based applications in the industries nowadays are developing more complex in construction, and the operations are being settled more efficient, reliable and user-friendly. However, the increasing load variations and the continuous usage of modern power electronic devices have pushed the motors into a fault-prone environment [1]. From the insight provided by the works of [2], possible failures could lead to severe monetary repercussions such as repair costs, unexpected shutdowns causing mass production delays and other less tangible factors, especially for industries. Since the applications above will keep on getting sophisticated in every sphere of life, for the excellent longevity of IMs, early motor faults diagnosis has become a predominant condition to the consumers in the competitive market of automation and drives.

Recent statistics given by [1] shows that IMs models contribute to approximately 80% of the component failure under all categories of faults, consequently generating interest in the importance of fault detection and monitoring of electric machinery over the recent years. From the study of IM faults, the most vulnerable parts to endure faults are bearing, stator windings, rotor bar and shaft. According to Karmarkar et al. [2], stator and rotor faults have been witnessed to occur during non-uniformity of air gap between stator-inner surface and rotor-outer surface. Moreover, IM faults are categorized into three categories:

- Electrical related faults under the classifications of the unbalanced voltage supply, reverse phase order, inter-turn short-circuits and overload.

- Mechanical related faults involving broken rotor bars, bearing damage, stator winding failure and air gap eccentricity.
- Environmental related faults include IM's performance affected by ambient temperature, external moisture, and machine vibrations due to installation defects.
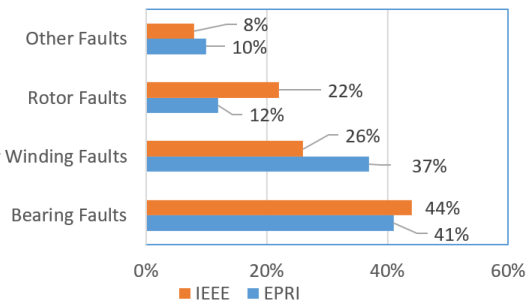

Fig. 1. IEEE and EPRI statistics on IM faults [1]

Regarding Fig. 1, stator windings fault and bearing faults form at least 60% of all IM faults. Humidity, partial discharge and mechanical stress are common reasons for the stator inter-turn fault (SITF). Literature [3]–[6] further discuss the factors behind the fault.

Stator winding faults are a common occurrence in IMs, and these faults occur when the coil windings are shorted with each other. The significant works of [7] include the detection of stator winding turn to turn fault, and the study also presents two methods to determine the severity of the fault. These methods are, first, neural-based estimators and, second, multi-agent systems (MAS). Furthermore, experimental evidence presented in the exact text concludes that winding faults of high severity are more accessible to detect than faults of low severity.

The proposed method in the works of [8] is used to detect stator inter-turn fault (SITF) and the broken rotor bar fault (BRBF) using MCSA. The dataset obtained from the faulty machine is compared with the same of a healthy motor. The Curvilinear Component Analysis (CCA) is chosen for Dimensionality Reduction (DR), and the paper favours this as a suitable method for representing non-linear datasets in comparison with linear methods such as Principal Component Analysis (PCA). CCA is chosen to perform two tasks, the first is to identify the data topology, whilst the second is to project the feature set (FS) into a lower dimension space (DR). Shallow Convolutional Neural Networks (SCNNs) are used for fault classification due to their robustness and simplicity.

Based on the experimental evidence in [9], SCNN has been deemed a superior classification technique compared to other types of classifiers discussed in this study. On the same note, Multilayer Perception Neural Network (MLP NN) is another good classifier used for multiple fault classification. The results presented by [10] show the effectiveness of the method in FD of an IM.

Another significant contribution seen in the work of [11] is the detection of harmonics using the prominence method. This technique returns the first nth prominent peaks of any frequency-based signal, and it is a more effective method in determining characteristic fault frequencies. Moreover, the prominence method has the upper hand over the maximum peak value measure since it can locate significant peaks throughout the signal spectrum rather than being inclined towards one side with a concentration of peaks. As such, the former is a better signal analysis tool.

So far, the methods explored in works of literature [11]–[16] have a common approach for FD of IMs. The generalized idea is to develop a mathematical model of the specific IM being tested, obtain data from the faulty machine and use feature extraction methods to find filter out data retaining only the valuable information. After that, Machine Learning (ML) algorithms are applied to train and test the system. However, the research done by [15] has a different standpoint altogether. The literature argues two significant points: firstly, the data-driven procedures require complex computations and mathematical modelling; secondly, these models can misdiagnose the faults caused by external factors such as motor misalignment or grid power imbalances.

The methods discussed in the above literature have either a model-driven or data-driven approach and, this approach has its strengths and weaknesses. However, irrespective of the path taken, they show promising results. The downside of the data-driven approach is that it is error-prone due to sensor misreading, and a considerable amount of pre-processing is required to clean and sort the data. On the other hand, the model-driven approaches cannot account for non-singularities and are limited by the known parameters. However, a mathematical model can be easily adjusted to simulate specific conditions, while the data-driven approach relies on machine data which can be noisy.

This paper aims to learn about the healthy and faulty conditions (SITF in particular) of an IM using the data generated by a model-based approach and how both kinds of conditions differ upon visualization. At first, the simulated data is generated by using the state-space model of a healthy and a faulty IM. Then, it is examined by using SVL and PCA techniques to detect the SITF class. The major interest lies in studying the SITF of very low severity (between 0.3% - 2%) using a linear technique, which most of the related studies have not presented so far. Finally, the evaluation of the SITF is carried out by studying the three-phase current signatures in 3D PCA planes. Following the successful detection and evaluation of SITF by PCA, this paper implies that it is possible to isolate the SITF (of very low severities) from the healthy three-phase current signature.

This paper is organized as follows: A generalized IM mathematical model is presented in section II, followed by the faulty IM model (for the SITF) in section III. Section IV represents the physical data of the IM used for generating data for SVL and PCA analysis. Section V demonstrates the simulated results using SVL and PCA together with discussions, and finally, the paper is concluded in section VI.

II. IM Model

The IM model consists of a squirrel cage stator with the symmetrical multiphase winding. This section contains the state space equations to realize an IM and is inspired by the works of [17]. These equations are realized in the synchronous reference frame to minimize analytical complexities when dealing with three-phase components.

Moreover, the SITF acts as an external stimulus and enhances the three-phase currents circulating in the IM. These additional currents are proportional to the severity of the fault and mainly influences the phase in which the shorting has occurred. Fig.2. shows the proposed scheme, in which the STIF is applied to a grid-connected three-phase squirrel cage induction motor. The resulting faulty three-phase currents are stored on a data frame from where they are accessed for PCA.
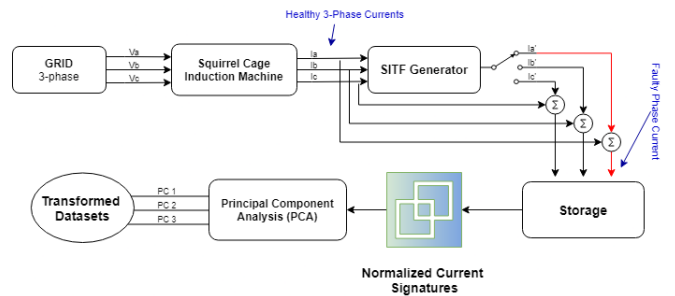

Fig. 2. Proposed scheme of IM with SITF and PCA

Representation of the Induction Motor in the mechanical reference frame, showing its state vector.

$$\dot{x} = Ax(t) + Bu(t) \tag{1}$$

$$\frac{d}{dt}\begin{bmatrix} i_s \\ \psi'_r \end{bmatrix} = \begin{bmatrix} A_{11} & A_{12} \\ A_{21} & A_{22} \end{bmatrix}\begin{bmatrix} i_s \\ \psi'_r \end{bmatrix} + \begin{bmatrix} B_1 \\ 0 \end{bmatrix} U_s \tag{2}$$

$$J\frac{dw_{rm}}{dt} + Bw_{rm} = T_{el} - T_L \tag{3}$$

$$i_s = Cx \tag{4}$$

where:

$$B = \frac{1}{(\sigma L_s)I} = bI, C = [I \quad 0], I = \begin{bmatrix} 1 & 0 \\ 0 & 1 \end{bmatrix} \text{ and, } J = \begin{bmatrix} 0 & -1 \\ 1 & 0 \end{bmatrix}$$

i_s and ψ'_r, stator current and rotor flux are the controllable states, B is the flux density on the rotor surface due to the stator currents, I is the Identity matrix and J is inertia coefficient matrix for the IM model. The model operates on Park's transformed voltages U_{sd} and U_{sq}.

The Inertia state matrix breakdown (A) is given by:

$$A_{11} = -\left\{\frac{R_s}{\sigma L_s} + \frac{1-\sigma}{\sigma T_r}\right\}I = a_{11} I \tag{5}$$

$$A_{12} = \frac{L_m}{\sigma L_s L_r \left\{\left(\frac{1}{T_r}\right)I - w_r J\right\}} = a_{12}\left\{\left(\frac{1}{T_r}\right)I - w_r J\right\} \tag{6}$$

$$A_{22} = -\left(\frac{1}{T_r}\right)I - w_r J = a_{22}\left\{\left(\frac{1}{T_r}\right)I - w_r J\right\} \tag{7}$$

$$A_{21} = \left\{\frac{L_m}{T_r}\right\}I = a_{21}I \tag{8}$$

Considering the direct-quadrature (DQ) axis reference representation matrix by using (1) and the breakdown matrices

of A, B, C above, a differential stator current and flux linkage in the DQ axis representation is defined as follows:

$$\frac{d}{dt}\begin{bmatrix} i_{sd} \\ i_{sq} \\ \psi_{sd} \\ \psi_{sq} \end{bmatrix} = \begin{bmatrix} a_{11} & 0 & \frac{a_{12}}{T_r} & a_{12}w_r \\ 0 & a_{11} & -a_{12}w_r & \frac{a_{12}}{T_r} \\ \frac{L_m}{T_r} & 0 & \frac{1}{T_r} & w_r \\ 0 & \frac{L_m}{T_r} & -w_r & \frac{1}{T_r} \end{bmatrix} \begin{bmatrix} i_{sd} \\ i_{sq} \\ \psi_{sd} \\ \psi_{sq} \end{bmatrix} + \begin{bmatrix} \frac{1}{\sigma L_s} & 0 \\ 0 & \frac{1}{\sigma L_s} \\ 0 & 0 \\ 0 & 0 \end{bmatrix} \begin{bmatrix} U_{sd} \\ U_{sq} \end{bmatrix} \quad (9)$$

Following is the IM model's mechanical speed Equation, T_{el} is the electro-magnet torque, p is the number of pair poles, B is the damping ratio in (10).

$$\dot{w_{rm}} = \frac{T_{el} - T_L - B\left(\frac{w_{rm}}{p}\right)}{J} \quad (10)$$

where the electro-magnetic torque and damping ratio breakdown are as follows:

$$T_{el} = \frac{\frac{3}{2}pL_m}{L_r}\left(i_{sd}\psi_{sq} - i_{sq}\psi_{sd}\right) \quad (11)$$

$$B = \frac{1}{\sigma L_s} \quad (12)$$

The remainder of the variables are constants whose values are machine specific. These are presented in Section IV.

II. FAULTY IM MODELLING

The SITF is described as the shorting between turns of the stator winding causing the production of additional current in the circuit.

The short-circuit winding, B_{cc}, produces a stationary magnetic field, H_{cc}, whose orientation is aligned according to the faulty winding. Meanwhile, the additional short-circuit current, i_{cc}, is an attribute of the short-circuit flux, ϕ_{cc}. Correspondingly, the voltage and flux equations also change due to these additional parameters. The changes are well explained in the works of [17], [18], and their state-space equations are used to model the SITF.

Theoretically, these additional currents are categorized as disturbances to the system, and in terms of state-space modelling, they are represented by the direct transition or feed-forward matrix.

The following equation describes the new output due to the presence of these disturbances.

$$y(t) = Cx(t) + Du(t) \quad (13)$$

where:
- $u(t)$, $y(t)$ and $x(t)$ are respectively the system input, output and state variables.
- C is the output matrix of constants

$$C = \begin{bmatrix} 1 & 0 & 0 & 0 \\ 0 & 1 & 0 & 0 \end{bmatrix} \quad (14)$$

- D is the direct transition matrix

$$D = \sum_{k=1}^{3} \frac{2n_{cck}}{3R_s} P(-\theta)Q(\theta_{cck})P(\theta) \quad (15)$$

Meanwhile, the direct transition (or feedforward) matrix is identified by the following variables:

- n_{cck} quantifies the SITF and is the ratio of the number of inter-turn short circuit winding in phase k and the number of turns in a healthy phase.
- θ_{cck} is 0 for phase A, $2\pi/3$ for phase B, and $4\pi/3$ for phase C
- R_s is the stator resistance which is obtained from the DC test results
- k is the phase containing the short-circuit and only accepted values are 1, 2 and 3 (denoting each phase)
- $P(\theta)$, $P(-\theta)$ and $Q(\theta cck)$ are respectively the Park, inverse Park and rotational matrices, respectively (16-17).

$$P(\theta) = \begin{bmatrix} \cos(\theta) & -\sin(\theta) \\ \sin(\theta) & \cos(\theta) \end{bmatrix} \quad (16)$$

$$Q(\theta_{cck}) = \begin{bmatrix} \cos(\theta_{cck})^2 & \cos(\theta_{cck})\sin(\theta_{cck}) \\ \cos(\theta_{cck})\sin(\theta_{cck}) & \sin(\theta_{cck})^2 \end{bmatrix} \quad (17)$$

III. IM PARAMETERS

The parameter extraction procedure is necessary to find the motor specific constants for modelling purposes. Moreover, they are found by performing the DC test, blocked rotor and no-load tests on the IM.

Table 1 lists the nameplate rating of the motor we used for our modelling, while table 2 details the IM parameters that were obtained through the tests.

TABLE 1: NAMEPLATE RATINGS

Rated Voltage	415V
Rated Current	4.6A
Frequency	50 Hz
Rated Speed	1500 rpm
Number Of Poles	4
Number Of Stator Slots	28
Number Of Rotor Slots	36
Type	B

TABLE 2: MACHINE PARAMETERS

Variable	Description	Value
R_S	Stator resistance	3.14Ω
R_e	Equivalent resistance	5.43Ω
R'_r	Referred rotor resistance	2.28Ω
Z_{SC}	Short circuit impedance	10.51Ω
X	Reactance of the motor	8.99Ω
X_s	Stator leakage reactance	5.39Ω
X'_r	Referred rotor reactance	3.59Ω
V_m	Magnetizing voltage	230.81V
I_i	Magnetizing current	0.36A
R_i	Resistance of the iron losses	633.39Ω
X_m	Magnetizing reactance	95.38Ω
L_m	Referred magnetizing inductance	0.3H
L_{sl}	Stator leakage inductance	0.02H
L'_{rl}	Referred rotor leakage inductance	0.04H
L_{ss}	Self-inductance of the stator	0.32H
L'_{rr}	Referred rotor self-inductance	0.22H
M_s	Stator mutual inductance	-0.1H
M'_r	Mutual inductance between rotor windings	-0.1H
M'_{sr}	Referred rotor-stator mutual inductance	0.2H
L_s	Stator inductance	0.41H
L'_r	Rotor referred inductance	0.32H
σ	Total leakage factor	0.14
T_r	Rotor time constant	0.14
L'_s	Stator transient inductance	0.06

IV. SIMULATION RESULTS

A. Analysis of the IM speed and torque responses under healthy and faulty scenarios

The rotational speed is the rate at which the rotor shaft rotates under voltage excitation. The following figure shows the speed response of the two models in rad/s. The settling time of the response is inversely proportional to the value of motor inertia (J), which is taken to be $0.02 kg/m^2$ for the healthy and faulty models, respectively.

In Fig. 3, the speed of the IM can be observed with no mechanical loading from 0 to 1.5 seconds. Both the models are subjected to 50% load from time equals 1.5 to 3 seconds. The healthy IM model's speed response settles within half a second with the IM's rated speed of 157.045 rad/s.

Similarly, the faulty IM model's speed with different severities approximately peaks to the same speed value as the healthy, but its settling time is slightly extensive than that of the healthy model's. It takes approximately 1 second for the faulty model to settle at the stable condition of w_m. For the corresponding Torque versus Time plots extracted at 50% load condition, the torque amplitude for healthy IM at simulation time of 2.3 seconds is 3.5 Nm, for the 0.7% faulty model at the same instance has a torque value of 3.64 Nm and 3.93 Nm for the 2.11% SITF model, respectively.

It should be noted that the torque responses for the faulty IMs at different severities generate large amounts of ripples. This is due to the harmonics generated electromagnetic torque due to non-idealities or faults in the electromagnetic fields produced by the stator interactions.
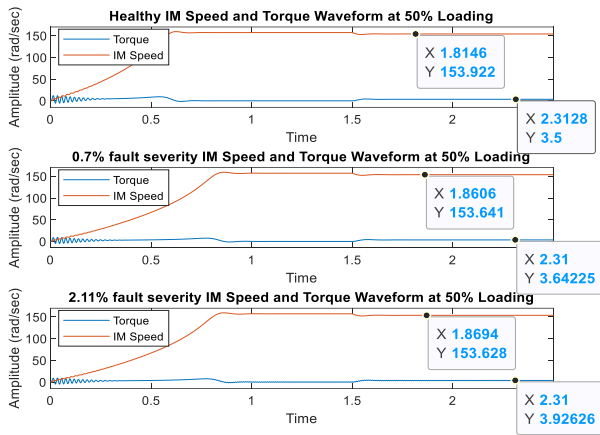

Fig. 3. Healthy and Faulty IM Speed Torque response plots

Following the above plots, the Speed-Torque curves of the IM can differentiate the healthy and faulty classes (Fig. 4). Even the smallest severity of SITF causes ripples in the torque signature when viewing from the x-axis. It can be noted that the increase of the fault severity increments the oscillation diameter in the plot (looking at the 0.3% to 2.11% fault severities). For the speed characteristics, its behaviour appears to be similar as in Fig. 3's response, i.e., the faults do not affect the IM speed response other than increasing the settling time.

B. Three-phase current analysis

The three-phase currents are visualized to understand the electrical impact of the SITF. As a result, it can be deduced that the severity of the fault is directly proportional to the amplitude of the three-phase current. Thus, this confirms that

the faulty phase should receive a higher current than its other two counterparts. This is because the SITF phenomenon lowers the resistance in the affected phase, causing unbalance, increasing the current value.
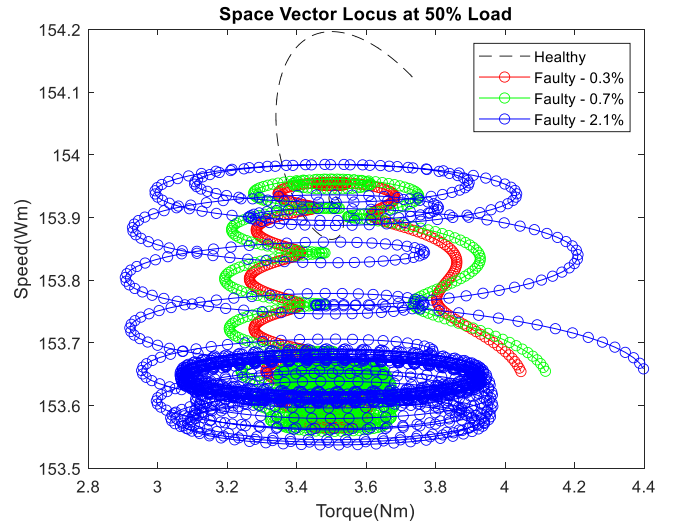

Fig. 4. IM Speed versus Torque Plot at 3.75 Nm Load

Fig. 5 shows the plots of the healthy IM model, faulty IM model with 0.7% severity (3-shorted turns) and 2.11% severity (6 shorted turns) accordingly. The three-phase current plot was extracted during the IM's 100% load (7 Nm) operation (using the IM model). The plots in Fig.2 are zoomed from 3.1 to 3.14 seconds. For the healthy three-phase current scenario, the peak values were measured to be 3.69A portraying a regular IM operation. The SITF was induced in phase A of the IM for the faulty model, where the generated abnormalities were detected from the other two phases— observing the Figs. 3-4. The three-phase currents of the faulty model have a visible spike in its phase A current signature compared to the current signatures of phases B and C.
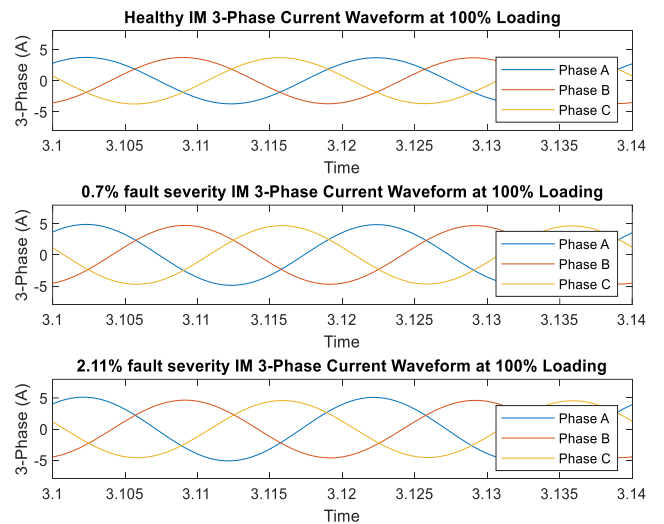

Fig. 5. Healthy and Faulty Induction Motor 3-Phase current response plots

Likewise, Fig. 6 clearly shows the separation between the healthy and faulty peak values of the current. In healthy phase A, the peak current is 3.67A, while for the SITF at 0.7% and 2.11%, the peak currents are 4.86A and 5.13A, respectively.
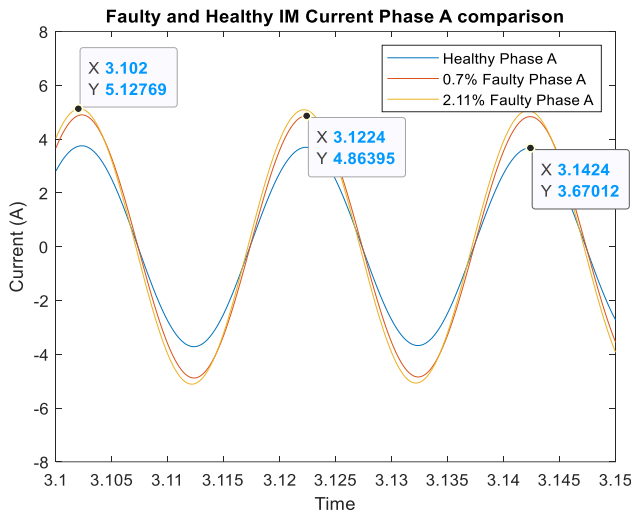
Fig. 6. Healthy and Faulty Induction Motor Phase A plots

C. DQ axis space-vector representation (SVL)

The space-vector representation (Fig. 7) shows the relationship between the direct and quadrature axis current at three scenarios: No Load, 50% Load (3.5Nm) and 100% Load (7Nm). Evaluating the DQ plot, firstly, the mechanical loadings variations on IM show the normal DQ current response as the system requires more current to anticipate the loadings, as portrayed in Fig. 7. This means that as the load increases, the radius of the SVL also increases.

The second observation is the shape of the SVL at different SITF severity levels. It can be deduced from Fig. 7 that as the fault severity increases, the respective SVL appear more distinctly elliptical and distanced from the healthy SVL. In the ideal case (which is for this simulation study), the healthy SVL is a perfect circle while the SITF SVL is elliptical as the severity increases.
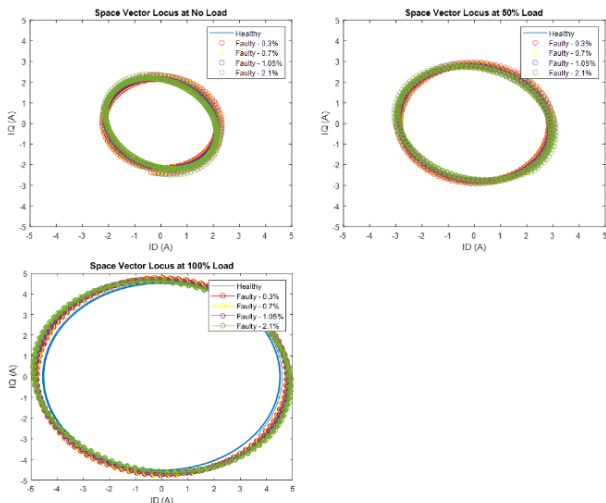

Fig. 7. Park's Current Vector for Healthy and Faulty IM Models

D. Principal component analysis of the faulty and healthy IM datasets

PCA is used as a measure of reducing the number of dimensions present in our dataset. Furthermore, the reduced dataset provides better insight in the data and the underlying relationship between them.

Figs. 8-9 illustrate the 2-dimensional and 3-dimensional views of the PCA plots. In the 2D PCA plot, the IM model

with the healthy and faulty scenarios shows the plot being shrunk and the data points clustered more on top of each other when the mechanical loading increases, retaining the similar elliptical shape seen in Fig. 7 (concerning healthy versus faulty case).
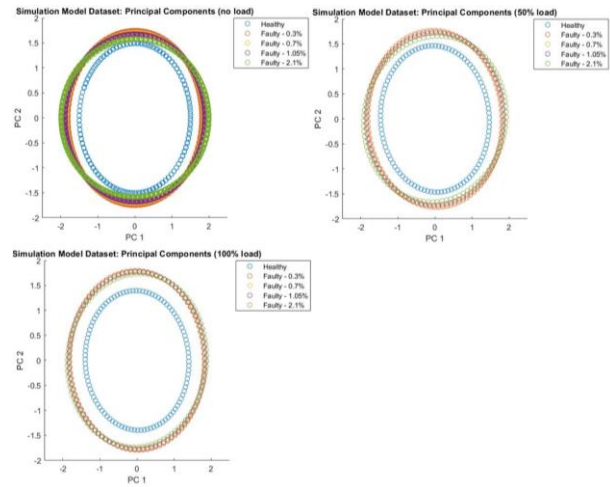

Fig. 8. Two Dimensional PC Plot of the Healthy and Faulty IM models at different loadings

As for the 3D view (Fig. 9), new observations can be made. All the five sets (healthy data and data with four different fault severities) of data points are elliptical when visualizing the PC1 (first PC) versus PC2 (second PC) axes. On the other hand, for PC1 and PC3 (third PC) axes, the healthy elliptical plot is approximately 30° from the PC3's positive axis. This angle increases even further as the models are subjected to higher loads. On the other hand, the faulty model's elliptical plots concerning the healthy plots seem to tilt closer to the PC3's positive axis. The faulty plot's angle in the PC3's negative axis seems to move further away. The main point noted from both the 2D and 3D PCA analyses is that the data points of a faulty model rotate in a clockwise direction about the PC2's axis as the SITF severity is incremented. Thus, this implies that PCA plots can distinguish the healthy signatures from faulty ones and can denote the changes in the fault severity. Compared with the SVL, which transforms the three-phase currents into DQ currents, PCA can also demonstrate the "elliptical" shape when it comes to the SITF. The PCA plot can also reflect the load change, but it can also reveal SITF severity variation through 3D plots.
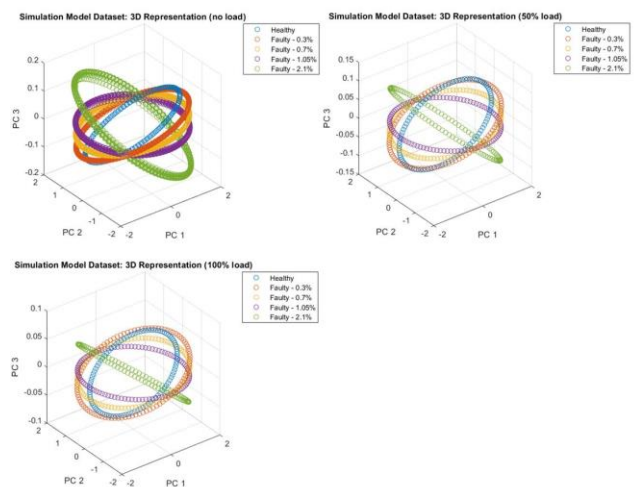

Fig. 9. Three Dimensional PC Plot of the Healthy and Faulty IM models at different loadings

V. CONCLUSION

This study has demonstrated that PCA, a linear dimensionality reduction technique, can also be used to detect and evaluate faults related to IMs. In particular, the study of SITFs for IMs and a state-space model was derived for a healthy and faulty IM. Using the simulated data, the objective of this study was to analyze the SITFs with very low severities. Thus, it comes to light that both SVL and PCA techniques can detect and follow the evolution of the SITF upon visualization. However, the latter is superior to the former and is instrumental in clearly identifying the SITF and its corresponding severity.

In addition, this study has also shown evaluation of the SITF at very low severities (0.3%-2.11%), which many studies have failed to highlight. The only drawback is that PCA is an unsupervised technique, whereby continuous monitoring of the motor operation and its corresponding analysis (PCA) is a factor. As a result, it is necessary to add an extra "classification" component to the current scheme to automate the alerting of the condition of the IM. Thus, this study serves the purpose of pre-processing the raw data via a linear-based technique, which, in the future, will be coupled with classical and state-of-the-art techniques to detect and evaluate the SITF severity in real time.

REFERENCES

[1] R. R. Kumar, G. Cirrincione, M. Cirrincione, A. Tortella, and M. Andriollo, "Induction Machine Fault Diagnosis Using Stator Current Subspace Spectral Estimation," in *2018 21st International Conference on Electrical Machines and Systems (ICEMS)*, Jeju, Oct. 2018, pp. 2565–2570. doi: 10.23919/ICEMS.2018.8549374.

[2] S. Karmakar, S. Chattopadhyay, M. Mitra, and S. Sengupta, *Induction Motor Fault Diagnosis*. Singapore: Springer Singapore, 2016. doi: 10.1007/978-981-10-0624-1.

[3] G. H. Bazan, P. R. Scalassara, W. Endo, A. Goedtel, R. H. C. Palacios, and W. F. Godoy, "Stator Short-Circuit Diagnosis in Induction Motors Using Mutual Information and Intelligent Systems," *IEEE Trans. Ind. Electron.*, vol. 66, no. 4, pp. 3237–3246, Apr. 2019, doi: 10.1109/TIE.2018.2840983.

[4] Y. Yagami, C. Araki, Y. Mizuno, and H. Nakamura, "Turn-to-turn insulation failure diagnosis of stator winding of low voltage induction motor with the aid of support vector machine," *IEEE Trans. Dielect. Electr. Insul.*, vol. 22, no. 6, pp. 3099–3106, Dec. 2015, doi: 10.1109/TDEI.2015.005198.

[5] H. A. Toliyat, S. Nandi, S. Choi, and H. Meshgin-Kelk, *Electric Machines: Modeling, Condition Monitoring, and Fault Diagnosis*, 1st ed. CRC Press, 2017. doi: 10.1201/b13008.

[6] B. Wang, C. Shen, K. Xu, and T. Zheng, "Turn-to-turn short circuit of motor stator fault diagnosis in continuous state based on deep auto-encoder," *IET Electric Power Applications*, vol. 13, no. 10, pp. 1598–1606, Oct. 2019, doi: 10.1049/iet-epa.2019.0101.

[7] R. H. C. Palacios, I. N. da Silva, A. Goedtel, W. F. Godoy, and T. D. Lopes, "Diagnosis of Stator Faults Severity in Induction Motors Using Two Intelligent Approaches," *IEEE Trans. Ind. Inf.*, vol. 13, no. 4, pp. 1681–1691, Aug. 2017, doi: 10.1109/TII.2017.2696978.

[8] R. R. Kumar, G. Cirrincione, M. Cirrincione, A. Tortella, and M. Andriollo, "A Topological and Neural Based Technique for Classification of Faults in Induction Machines," in *2018 21st International Conference on Electrical Machines and Systems (ICEMS)*, Jeju, Oct. 2018, pp. 653–658. doi: 10.23919/ICEMS.2018.8549509.

[9] S. Munikoti, L. Das, B. Natarajan, and B. Srinivasan, "Data-Driven Approaches for Diagnosis of Incipient Faults in DC Motors," *IEEE Trans. Ind. Inf.*, vol. 15, no. 9, pp. 5299–5308, Sep. 2019, doi: 10.1109/TII.2019.2895132.

[10] R. R. Kumar, G. Cirrincione, M. Cirrincione, M. Andriollo, and A. Tortella, "Accurate Fault Diagnosis and Classification Scheme Based on Non-Parametric, Statistical-Frequency Features and Neural Networks," in *2018 XIII International Conference on Electrical Machines (ICEM)*, Alexandroupoli, Sep. 2018, pp. 1747–1753. doi: 10.1109/ICELMACH.2018.8507213.

[11] S. B. Jiang, P. K. Wong, and Y. C. Liang, "A Fault Diagnostic Method for Induction Motors Based on Feature Incremental Broad Learning and Singular Value Decomposition," *IEEE Access*, vol. 7, pp. 157796–157806, 2019, doi: 10.1109/ACCESS.2019.2950240.

[12] R. R. Kumar, G. Cirrincione, M. Cirrincione, A. Tortella, and M. Andriollo, "A Topological Neural-Based Scheme for Classification of Faults in Induction Machines," *IEEE Trans. on Ind. Applicat.*, vol. 57, no. 1, pp. 272–283, Jan. 2021, doi: 10.1109/TIA.2020.3032944.

[13] S. Munikoti, L. Das, B. Natarajan, and B. Srinivasan, "Data-Driven Approaches for Diagnosis of Incipient Faults in DC Motors," *IEEE Trans. Ind. Inf.*, vol. 15, no. 9, pp. 5299–5308, Sep. 2019, doi: 10.1109/TII.2019.2895132.

[14] S. B. Jiang, P. K. Wong, and Y. C. Liang, "A Fault Diagnostic Method for Induction Motors Based on Feature Incremental Broad Learning and Singular Value Decomposition," *IEEE Access*, vol. 7, pp. 157796–157806, 2019, doi: 10.1109/ACCESS.2019.2950240.

[15] B. Devi Sekar and M. C. Dong, "Bayesian fuzzy inference nets online fault diagnosis of induction motor," in *2009 7th International Conference on Information, Communications and Signal Processing (ICICS)*, Macau, China, Dec. 2009, pp. 1–5. doi: 10.1109/ICICS.2009.5397664.

[16] L. A. Garcia-Escudero, "Robust Detection of Incipient Faults in VSI-Fed Induction Motors Using Quality Control Charts," *IEEE TRANSACTIONS ON INDUSTRY APPLICATIONS*, vol. 53, no. 3, p. 10, 2017.

[17] S. Bachir, S. Tnani, J.-C. Trigeassou, and G. Champenois, "Diagnosis by parameter estimation of stator and rotor faults occurring in induction machines," *IEEE Trans. Ind. Electron.*, vol. 53, no. 3, pp. 963–973, Jun. 2006, doi: 10.1109/TIE.2006.874258.

[18] B. Saddam, B. S. Ahmed, A. Aissa, and T. Ali, "Squirrel Cage Induction Motor under Stator and Rotor Bars Faults Modeling and Diagnosis," in *2018 International Conference on Communications and Electrical Engineering (ICCEE)*, El Oued, Algeria, Dec. 2018, pp. 1–6. doi: 10.1109/CCEE.2018.8634502.

[19] S. Marmouch, T. Aroui, and Y. Koubaa, "Induction machine faults diagnosis by statistical neural networks with selection variables based on Principal component analysis," in *2017 18th International Conference on Sciences and Techniques of Automatic Control and Computer Engineering (STA)*, Monastir, Dec. 2017, pp. 99–103. doi: 10.1109/STA.2017.8314887.